NUMERICAL SIMULATION OF DAMAGE IN THERMOPLASTIC COMPOSITE MATERIALS

Kevin Brown[1], Richard Brooks, Nicholas Warrior

School of Mechanical, Materials and Manufacturing Engineering
University of Nottingham
University Park
Nottingham NG7 2RD
UK

Keywords:
Thermoplastic composites, explicit finite element analysis, damage mechanics, impact

[1] Corresponding author; Tel: 44 (0) 115 8466443; Fax: 44 (0) 115 8466771; E-mail: eaxkab@nottingham.ac.uk

ABSTRACT

Thermoplastic composites are being considered for application in vehicle bumper and front-end structures for increased pedestrian protection. This paper describes recent progress in the calibration and validation of LS-DYNA™ material model 162 (*MAT_COMPOSITE_DMG_MSC) for the modelling of impact damage in the glass/polypropylene commingled fabric thermoplastic composite, Twintex™. In this study, MAT 162 is calibrated by using a series of tests that were conducted at quasi-static and dynamic loading rates. These consisted of in-plane tension, shear and compression tests. A novel procedure for calibrating in-plane shear damage is presented. To demonstrate the predictive capabilities of the model, the response of Twintex™ laminates subject to dynamic impact loading is simulated. The force–time histories and damage predictions are successfully compared with corresponding experimental instrumented falling weight test results. It is concluded that MAT 162 provides a versatile tool for predicting damage progression in thermoplastic composites.

INTRODUCTION

Vehicle manufacturers are faced with the challenge of designing new bumper systems and front-end structures to meet the soon to be introduced European Commission (EC) pedestrian safety legislation [1]. This has increased interest in the application of thermoplastic composites in vehicle bumper and frontal structures for improved pedestrian protection. These materials are already being used for both primary and secondary vehicle components due to their prominent physical and mechanical properties, in addition to high volume processability and recyclability. However, before these materials can be optimally applied to pedestrian safety in vehicles, a greater understanding of their impact damage and energy absorption characteristics is required. There have been numerous studies on impact loading and damage in thermoset composites. However, very little work has been done on the assessment of impact damage in thermoplastic composites using finite element analysis techniques.

This paper describes the application of the MAT 162 composite material model within LS-DYNA™ to simulate impact damage in a thermoplastic composite. The thermoplastic composite of interest in this study is Twintex™ (T PP 60 745 AF), which is a balanced commingled E-glass and polypropylene woven fabric composite supplied by Saint Gobain Vetrotex. A brief description of MAT 162 is presented first, followed by a description of the calibration and validation methodology. The paper concludes with a discussion of the results.

LS-DYNA™ MATERIAL MODEL 162

A detailed description of MAT 162 is given in [2]. However, for completeness a brief description is provided below.

MAT 162 (*MAT_COMPOSITE_DMG_MSC) is based on the Matzenmiller et al [3] continuum damage mechanics (CDM) formulation. Damage progression is characterised by decreasing the material stiffness during post-failure. The stiffness reduction is expressed in terms of the associated damage parameter, ω_i:

$$E_i = (1 - \omega_i)E_i^0 \quad (1)$$

$$\omega_i = 1 - \exp\left(\frac{-r_i^{m_j}}{m_i}\right) \qquad r_i \geq 1 \quad i = 1,...,6 \qquad j = 1,\ldots,4 \quad (2)$$

Where E_i^0 are the initial elastic modulii, E_i are the reduced elastic modulii, r_i are the damage thresholds that are governed by six failure criteria and m_j are the four material damage parameters: $m_{f,x}$ (fibre damage in x-direction), $m_{f,y}$ (fibre damage in y-direction), $m_{crsh,shr}$ (fibre crush and punch shear), $m_{m,delm}$ (matrix and delamination). The damage variable, ω_i, ranges from 0 (no damage) to 1 (complete failure).

The effect of strain rate on lamina properties is modelled by semi-logarithmic functions:

For rate dependent strength properties:

$$\{S_{rt}\} = \{S_0\}\left(1 + C_1 \ln \frac{\left\{\dot{\varepsilon}\right\}}{\dot{\varepsilon}_0}\right) \quad (3)$$

Where C_1 is the strain rate constant for strength properties, $\{S_0\}$ are the quasi-static reference strength values, $\{S_{rt}\}$ are the rate dependent strength values, $\dot{\varepsilon}_0$ is the quasi-static reference strain rate value, and $\left\{\dot{\varepsilon}\right\}$ are the associated strain rates

For rate dependent stiffness properties:

$$\{E_{rt}\} = \{E_0\}\left(1 + C_i \ln \frac{\left\{\dot{\varepsilon}\right\}}{\dot{\varepsilon}_0}\right) \qquad i = 2,\ldots,4 \quad (4)$$

Where C_i are the strain rate constants for elastic modulii (C_2 – longitudinal modulii, C_3 – shear modulii, C_4 – transverse modulii), $\{E_0\}$ are the quasi-static reference strength values, and $\{E_{rt}\}$ are the rate dependent strength values.

METHODOLOGY

The numerical methodology that is described in this paper consists of two phases: 1) quasi-static material calibration and validation followed by 2) dynamic impact material damage validation and predictive analysis.

Quasi-Static Material Calibration

Calibration of MAT 162 was performed using a series of quasi-static uniaxial coupon tests ($[090]_{8fs}$ tension, $[\pm45]_{8fs}$ shear and $[090]_{8fs}$ compression). These tests provided the elastic, strength and damage properties for Twintex™. However, there is no clearly defined method for calibrating damage growth and post-failure softening [4]. As a first step, a single solid element loaded in tension was used to observe the effect of different values of m_j on the predicted post failure response and subsequent damage evolution in Twintex™. Figure 1 shows that as m_j decreases, the post-

failure softening and damage evolution becomes more gradual, while abrupt failure occurs at high values of m_j (e.g. m = 10). These qualitative observations were used as a guide in selecting values of m_j for more detailed finite element models of the calibration tests.

For the $[090]_{8fs}$ tension and $[090]_{8fs}$ compression models, damage parameters, $m_{f,x}$ and $m_{f,y}$ were set to a value of 4 to represent the abrupt fibre failure observed in these tests. Figures 2 and 3 show good agreement between the predicted stress-strain response and the experimental results for both tension and compression respectively.

However, selecting a value for the shear damage parameter, $m_{m,delm}$, is not as straightforward. The $[\pm45]_{8fs}$ in-plane shear tests yielded a non-linear 'hardening' stress-strain response. The strategy for calibrating the shear response included approximating the non-linear stress-strain curve to a bi-linear fit, line A-B-C, as shown in Figure 4. Section A-B is the initial elastic response. The post-elastic 'hardening' (section B-C) was invoked by selecting the stress at transition point B as the shear strength, $S_{xy.}$ Different values of $m_{m,delm}$ were assessed with -0.15 giving the best representation of the post-failure shear response. Using this methodology, Figure 5 shows good general correlation between the non-linear experimental shear stress-strain response and the simulation results. However, it must be noted that the transition from the elastic region to non-linear hardening occurs more abruptly in the predicted plot.

Quasi-Static Validation

Two test examples were employed for validation of MAT 162 for in-plane quasi-static loading, $[0/90]_{8fs}$ in-plane tensile hole-in-plate and $[\pm45]_{8fs}$ in-plane tensile hole-in-plate. The experimental data for the validation tests was taken from Wilson [5]. Finite element models with a fine and coarse mesh discretisation were developed for these tests. Predicted stress-strain curves and damage were compared to the experimental results.

$[090]_{8fs}$ in-plane tensile hole-in-plate test simulation

Good correlation is observed between the experimental and predicted stress-strain results for both discretisations as depicted in Figure 6. The peak load is underestimated; however, the post-failure softening is captured very well by the fine mesh. Figure 7 (a) – (d) shows the predicted fibre fracture, matrix damage, and delamination for the fine mesh at 2.5 % strain. The general macroscopic damage predictions correlate well with the observed damage. The predicted damage did not show significant mesh sensitivity.

$[\pm45]_{8fs}$ in-plane tensile hole-in-plate test simulation

Figure 8 shows that the non-linearity in the experimental stress-strain plot is captured by the predicted results. However, the fine mesh result deviates from the experimental curve at a strain value of about 5 % due to the onset of element erosion. Figure 9 shows the predicted damage for the fine mesh. In-plane damage initiates at 1.3 % strain with damage occurring along the fibre orientation angle (45°). This corresponds well with the experimental observations. However, at 5 % strain, in-plane matrix damage is predicted along the whole length of the specimen for both mesh densities. This is not representative of the actual tests. The 'necking' that is

shown in Figure 9 (c) for the fine mesh corresponds well with the experimental results.

Dynamic Impact Damage Simulation

The ability of MAT 162 to predict damage caused by low velocity impact was evaluated by simulating a series of experimental falling weight impact tests on Twintex™ at incident energy levels of 30, 35, and 45 J (Santulli et al [6]). The Twintex™ plates (80 mm x 80 mm) had a stacking sequence of $[0/90]_{8fs}$ with a nominal thickness of 4 mm and were clamped under a circular anvil with a 40 mm diameter. Impact was imparted by 25.65 kg striker with a 12.7 mm diameter hemispherical tip. Figure 10 (a) shows a schematic of the impact test setup. Damage was assessed using an Agema Thermovision 900 infrared thermography camera [6].

The finite element model for the falling weight impact test simulations is shown in Figure 10 (b). Geometric and material symmetry allowed one-half of the impactor and plate to be modelled which saved computational time. The Twintex™ plate was modelled using one solid element per ply with a refined mesh in the impact area. The outer boundaries of the plate were considered to be clamped, while symmetric conditions were applied to the symmetric plane. The impactor was treated as a rigid material (MAT_RIGID) with the elastic and strength properties of steel. Contact between the plate and the impactor was modelled using the ERODING_SINGLE_SURFACE contact algorithm. Element erosion was given by fiber failure to avoid excessive distortion of the failed elements. All failed elements were deleted and the contact surfaces were updated to the adjacent layers of the material. A stiffness based (type 4) hourglass control was employed to improve the deformation behaviour of the elements.

The material properties and parameters used in the impact simulations are given in Table 1. Two sets of values for the damage parameters were used in the impact analysis in order to observe their effect on the predicted results (see Table 2). In Case 1 the calibration damage values obtained from the quasi-static in-plane analysis described above were applied, while in Case 2, all the damage parameters were set to a value of 1, except for the value of $m_{m,delm}$ which remained at -0.15 in both Cases. The strain rate input parameters for MAT 162 as described above were obtained from dynamic tensile, shear and compression tests that were conducted in a falling weight drop tower using specially designed fixtures. Detailed results for these tests are to be published at a later date.

Results

Figure 11 shows comparison between the experimental and predicted force-time history plots for the 30 J event. For both Cases 1 and 2, the peak force is over-predicted by about 15 %; however, the overall shape of the predicted curve is similar to the experimental results.

Figures 12 and 13 show a comparison between the experimental and predicted force-time history plots for the 35 J and 45 J impact events respectively. It is clear that the damage parameters used in Case 2 results in a better correlation between the predicted and experimental force-time history plots. For Case 1, the predicted force-time plots show a significant drop in the contact force at about 0.008 s which deviates from the experimental plot. This was due to the more abrupt failure that

occurs with m_j values of 4 (Case 1) subsequently resulting in excessive element erosion in the impact area.

Figures 14 and 15 show the predicted in-plane and through-thickness matrix damage for Cases 1 and 2 respectively compared with the thermography measurements.
For both Cases 1 and 2 damage predictions are localised in the central region of the plate which agrees well with the test observations. In addition, there is no significant difference between the size of the damage region for both Cases. However, at the higher energy of 45 J, Case 1 predicts penetration of the plate which does not occur in practice. Again, this appears to be a consequence of the higher values of m_j (= 4) resulting in abrupt failure and element erosion. Case 2 clearly gives better representation of the post failure damage. These results indicate that improved simulations will be achieved by supplementing the coupon level material calibrations with a baseline dynamic impact calibration to ensure damage progression is mapped correctly.

SUMMARY AND CONCLUSIONS

In this study, MAT 162 has been successfully calibrated and validated for modelling impact damage in the thermoplastic composite, Twintex™. A practical calibration methodology was presented which included a novel procedure for calibrating non-linear shear damage. This study has shown that calibration of damage parameters from uniaxial coupon test data provides reasonable predictions of impact damage. However, improved predictions can be potentially obtained by numerically calibrating the damage parameters using a baseline dynamic impact simulation. These same calibrated damage values may then be used in simulating the behaviour of the same laminate under different impact conditions. Future work includes further component level validation of the predictive capabilities of MAT 162 for thermoplastic composite structures

ACKNOWLEDGEMENTS

The authors would like to thank Saint-Gobain Vetrotex for the supply of Twintex™ material. We would also like to acknowledge support from the UK Engineering and Physical Sciences Research Council (EPSRC) through the Nottingham Innovative Manufacturing Research Centre (NIMRC). The authors are grateful to Dr. Martin Wilson for providing experimental data.

REFERENCES

1. *Directive 2003/102/EC of the European Parliament and Council relating to the protection of pedestrians and other vulnerable road users*. http://europa.eu.int/comm/enterprise/automotive/pagesbackground/pedestrianprotection/index.htm.
2. Hallquist, J.O., *LS-DYNA Keyword User's Manual Version 970*. 2003, Livermore: Livermore Software Technology Corporation.
3. Matzenmiller, A., J. Lubliner, and R.L. Taylor, *A constitutive model for anisotropic damage in fiber-composites.* Mechanics of Materials, 1995. **20**(2): p. 125-152.
4. Williams, K. and R. Vaziri. *Finite Element Analysis of the Impact Resonse of CFRP Composite Plates*. in *Proceedings of ICCM 10*. 1995. Whistler, B.C., Canada.

5. Wilson, M., *Finite Element Analysis of Glass Fibre Reinforced Thermoplastic Composites for Structural Automotive Components*, in *PhD Thesis*. 2003, The University of Nottingham: Nottingham.
6. Santulli, C., et al., *Impact Properties of Compression Moulded Commingled E-glass Polypropylene Composites.* Plastics, Rubber and Composites, 2002. **31**(6): p. 270-277.

Table 1. Material properties used for impact analysis for Twintex™ 1:1

Properties	Value
Density, ρ	1500 kg/m^3
Modulus, E_x , E_y	14 GPa
Through-thickness Modulus [a], E_z	5.3 GPa
In-Plane Shear Modulus, G_{xy}	1.79 GPa
Out-Plane Shear Modulus [a], G_{xz}, G_{yz}	1.52 GPa
Poisson's Ratio [a], v_{xy}	0.08
Poisson's Ratio [a], v_{xz}	0.14
Poisson's Ratio [a], v_{yz}	0.15
Tensile Strength, S_{xT} , S_{yT}	269 MPa
Compression Strength, S_{xC}, S_{yC}	178 MPa
Through-Thickness Tensile Strength [b], S_{TT}	100 MPa
Crush Strength [b], S_{crsh}	300 MPa
Through-Thickness Shear Strength, S_{xz}, S_{yz}	120 MPa
Shear Strength [c], S_{xy}, S_{xz}, S_{yz}	22 MPa
Coulomb friction angle [b], ø	20
Delamination Scale Factor, S	1.0
Strength Properties Strain Rate Coefficient, C_1	0.024
Longitudinal Modulii Strain Rate Coefficient, C_2	0.0066
Shear Modulii Strain Rate Coefficient, C_3	-0.07
Transverse Modulii Strain Rate Coefficient, C_4	0.0066

[a] Wilson [5]
[b] Estimated values
[c] Based on transition point on bi-linear fit for shear stress-strain experimental curve as explained in text above

Table 2. Calibration damage parameters for impact simulations

Damage parameters	Case 1	Case 2
Fibre damage	$m_{f,x} = m_{f,y} = 4$	$m_{f,x} = m_{f,y} = 1$
Fibre crush and punch shear	$m_{crsh,sh} = 4$	$m_{crsh,sh} = 1$
Matrix and delamination	$m_{m,delm} = -0.15$	$m_{m,delm} = -0.15$

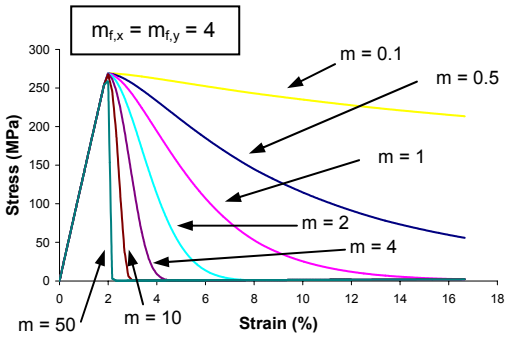

Figure 1. Effect of the damage exponent on the predicted longitudinal stress-strain response for Twintex™

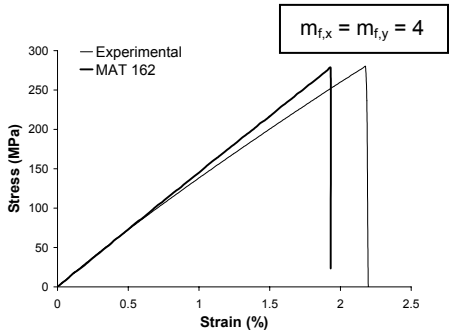

Figure 2. Predicted and experimental stress-strain response for $[090]_{8fs}$ tension calibration simulation

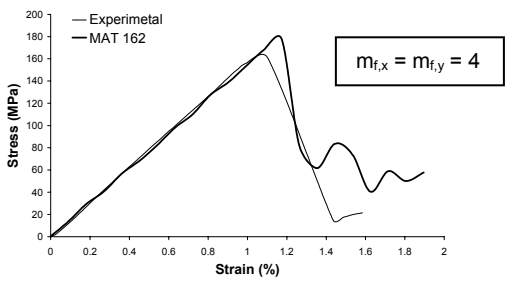

Figure 3. Predicted and experimental stress-strain response for $[090]_{8fs}$ compression calibration sim ulation

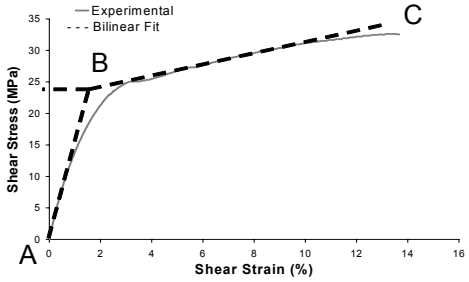

Figure 4. Showing bi-linear fit curve (line A-B-C) for calibrating in-plane shear

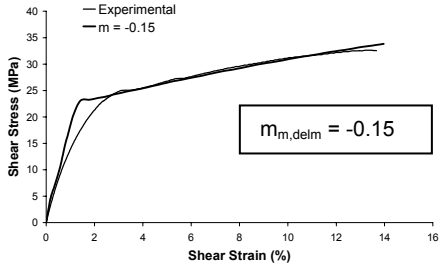

Figure 5. Predicted and experimental stress-strain response for $[\pm 45]_{8fs}$ in-plane shear calibration simulation

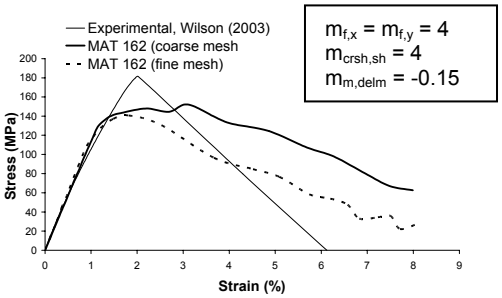

Figure 6. Predicted and experimental stress-strain response for $[090]_{8fs}$ tensile hole-in-plate validation simulation

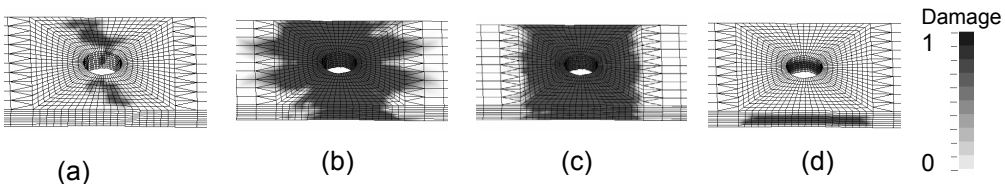

Figure 7. Fine mesh predicted damage for $[090]_{8fs}$ tensile hole-in-plate simulation at strain = 2.5 % (a) fibre fracture in x-direction (b) in-plane matrix damage (c) thru-thickness matrix damage (d) delamination

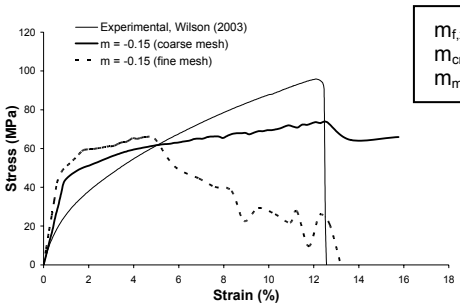

Figure 8. Comparison of predicted and experimental stress-strain response for 45 tensile hole-in-plate validation simulation

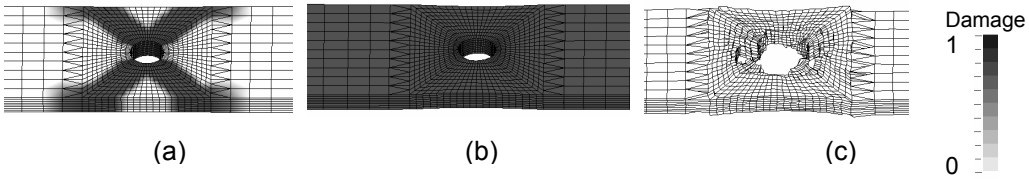

Figure 9. Fine mesh predicted damage for $[\pm 45]_{8fs}$ tensile hole-in-plate simulation (a) in-plane matrix damage at strain = 1.3 % (b) in-plane matrix damage at strain = 5 % (c) failed shape at strain = 11.3 %

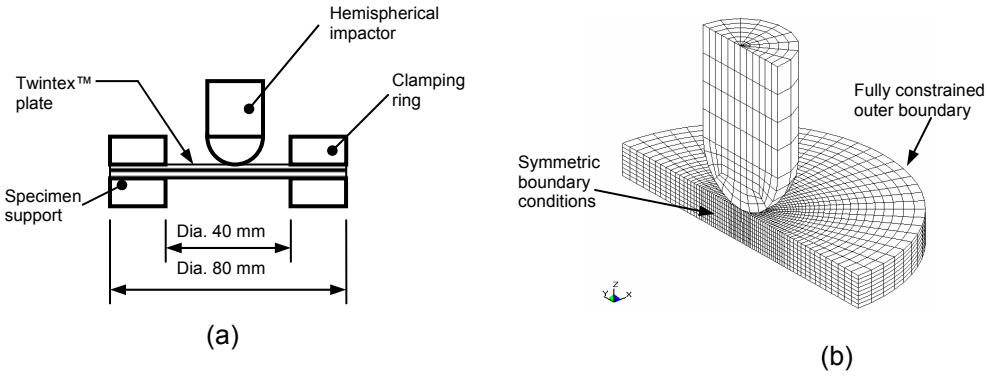

Figure 10. Falling weight impact test (a) schematic of the test setup (b) finite element model

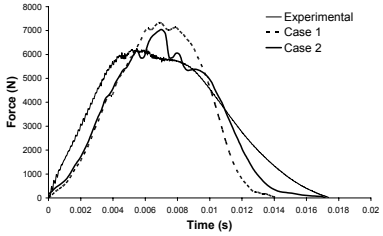

Figure 11. Showing experimental and predicted force-time responses for a 30 J impact on a $[090]_{8fs}$ Twintex Plate

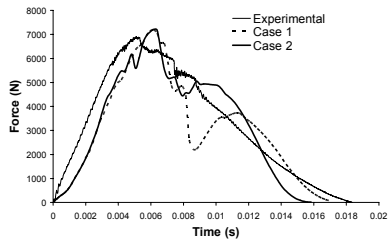

Figure 12. Showing experimental and predicted force-time responses for a 35 J impact on a $[090]_{8fs}$ Twintex Plate

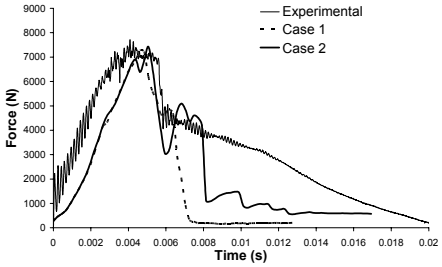

Figure 13. Showing experimental and predicted force-time responses for a 45 J impact on a $[090]_{8fs}$ Twintex Plate

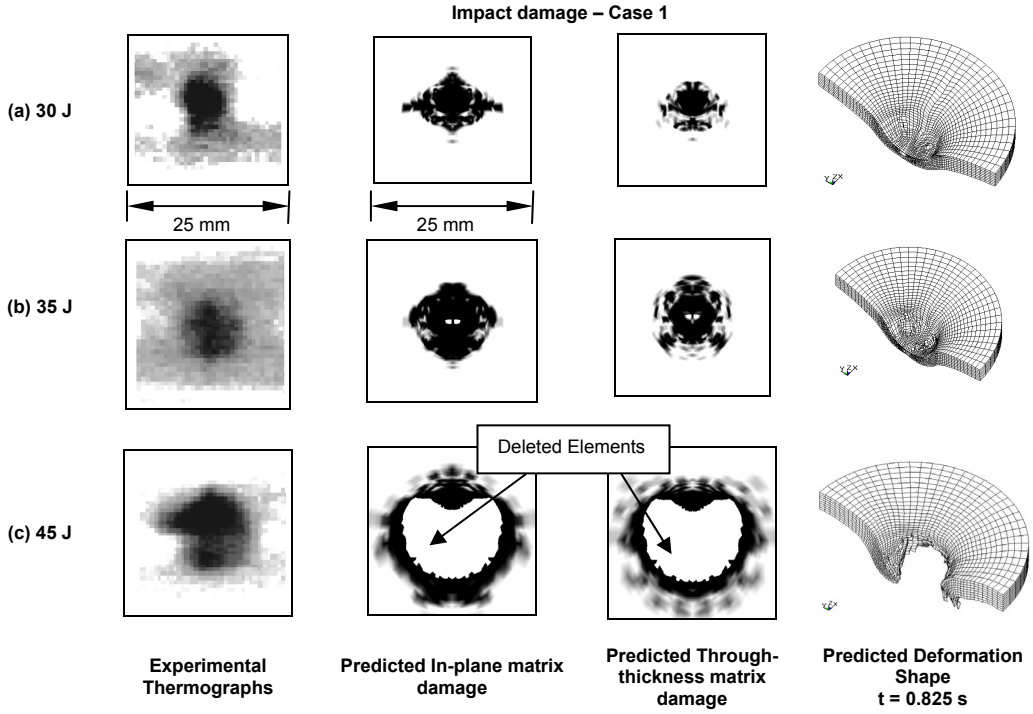

Figure 14. Comparison of predicted in-plane and through-thickness damage on the middle ply and experimental thermographs for impact events on a $[090]_{8fs}$ Twintex™ plate for Case 1

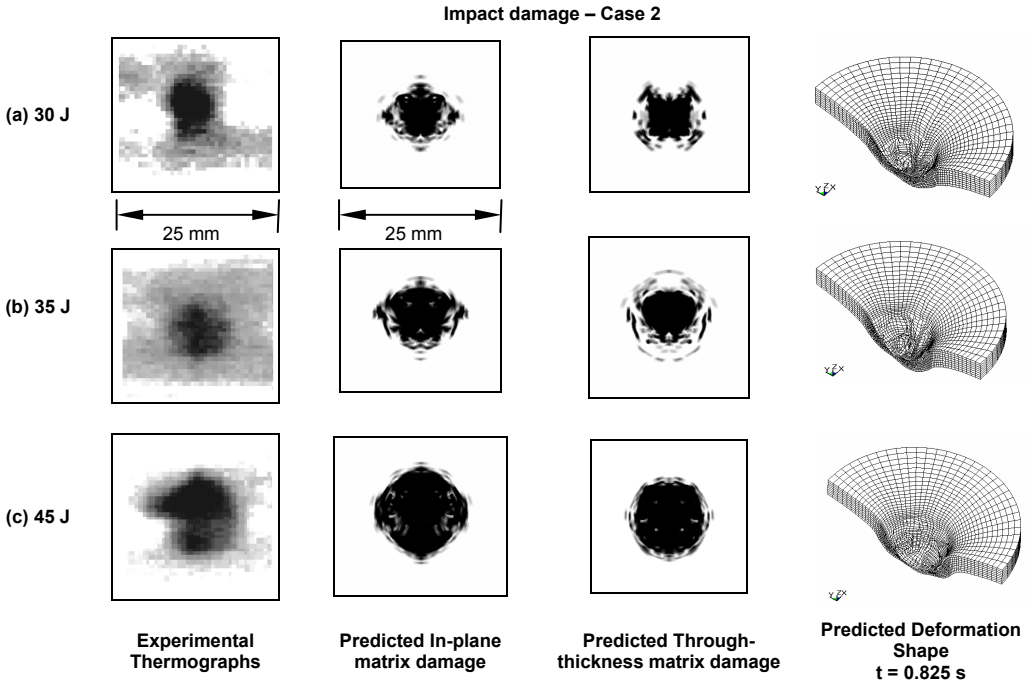

Figure 15. Comparison of predicted in-plane and through-thickness damage on the middle ply and experimental thermographs for impact events on a $[090]_{8fs}$ Twintex™ plate for Case 2